Dr. Mario Passeggi.

ChemPubSoc Europe

DOI: 10.1002/ejic.201800593

EurJIC European Journal of Inorganic Chemistry

Full Paper

Magnetic Exchange Interactions

Coupled High Spin Co^{II} Ions Linked by Symmetrical Double Hydrogen Bonds: Role of a Slowly Relaxing Cu^{II} Impurity in Interrupting the Co^{II}–Co^{II} Exchange Interaction

Ana L. Pérez,[a] Axel Kemmerer,[a] Marilin A. Rey,[a] Sergio D. Dalosto,[b] Carlos A. Ramos,[c] Mario C. G. Passeggi,[a,b] Alberto C. Rizzi,[a] and Carlos D. Brondino *[a]

Abstract: Co^{II} and Cu^{II} ions are two paramagnetic transition metal ions showing different relaxation rates (ν), with $\nu_{Co}{}^{II}$ >> $\nu_{Cu}{}^{II}$. To measure the isotropic exchange constant (J) between high spin Co^{II} ions and between Cu^{II} ions and high spin Co^{II} ions, we performed magnetic and EPR measurements complemented with computational calculations on pure *trans*-diaqua-bis(picolinato-*N*,*O*)-cobalt(II) dihydrate (**1**), on the Cu^{II} ion doped compound of **1 (2)**, and on the Cu^{II} ion doped compound in a Zn^{II} matrix isomorphous to **1**. The temperature dependence of the Cu^{II} EPR resonance lines of **2** induced by the fast relaxing Co^{II} ion host as well as the evaluation of the temperature-independent Co^{II}–Co^{II} and Cu^{II}–Co^{II} isotropic exchange interaction are analyzed. We determined an antiferromagnetic interaction [J_{Co-Co} = −1.07(1) cm^{-1}] associated with a double symmetrical hydrogen bond bridge and another one [$|J|_{Co-Cu}$ = 0.0015(2) cm^{-1}] associated with a double but asymmetrical hydrogen bond bridge, which are in line with the values obtained from computational calculations. This work shows that EPR spectroscopy can advantageously be used to evaluate weak exchange interactions between distinct metal ions with different relaxation rates by using the fact that those metal–metal interactions that broaden the EPR resonance line, which are described by matrices with a trace of zero, are averaged out at high temperatures.

Introduction

Understanding of magnetic properties of paramagnetic solid state transition ion coordination compounds is mandatory to gain insight on the metal–metal interactions and how the single ion magnetic properties contribute to the overall magnetic behavior of the system.[1] The crystal lattices of these compounds present mononuclear or oligonuclear metal centers, that usually present inter-center through-distance and through-bond interactions which give rise to extended interactions. The magnetic properties of these systems are governed by those extended interactions, but in some cases the molecules that connect the metal ions shield the magnetic centers, in such a way that make inter-center interactions almost negligible. Magnetic measurements and electron paramagnetic resonance (EPR) are two techniques that have widely been used to characterize paramagnetic solid state compounds with magnetic properties determined by extended interactions;[2] the former is principally used for evaluating zero field splitting (ZFS) parameters and exchange coupling constants (J) among metal centers larger than 1 cm^{-1} ($H_{ex} = -J\ S_1 \cdot S_2$), whereas the latter, particularly when applied to single crystal samples, has been used to evaluate the matrices associated with anisotropic interactions (e.g. Zeeman and hyperfine interactions) and isotropic exchange coupling constants smaller than 1 cm^{-1}.[1d,3] Both kind of studies are generally performed on pure compounds, which in some cases make it difficult the analysis because of the relatively large number of interactions that must be taken into account. This difficulty may be overcome by using diamagnetic host compounds isomorphous to the pure one doped with magnetic impurities, which pursues to isolate the magnetic center from its nearest magnetic neighbors.[4] The combined use of these experimental techniques complemented with computational calculations have become powerful tools to characterize not only the essential blocks that form a magnetic material, but also to extract information on the chemical pathways responsible for transmitting the above mentioned through-bond extended interactions. Furthermore, despite these studies are performed on solid state compounds, they are also of interest in the study of metal containing biological systems, as the essential blocks and superexchange pathways of the solid state compounds may show resemblances with those found in redox metalloenzymes and electron transfer proteins.[5] In other words, though metal centers in biological and solid state paramagnetic compounds may have very well differentiated roles, they present common features that can be used

[a] *Departamento de Física, Facultad de Bioquímica y Ciencias Biológicas, Universidad Nacional del Litoral - CONICET, Ciudad Universitaria, S3000ZAA Santa Fe, Argentina*
E-mail: brondino@fbcb.unl.edu.ar
www.fbcb.unl.edu.ar/dfbioq
[b] *Instituto de Física del Litoral, Universidad Nacional del Litoral - CONICET, Güemes 3450, 3000 Santa Fe, Argentina*
[c] *Centro Atómico Bariloche, Comisión Nacional de Energía Atómica, Av. Bustillo 9500, 8400 Bariloche, Río Negro, Argentina*
Supporting information and ORCID(s) from the author(s) for this article are available on the WWW under https://doi.org/10.1002/ejic.201800593.

to learn on the function and structure of these metal centers within the systems they are embedded.[6]

Considerable efforts in the field have been devoted to study paramagnetic heterometallic compounds,[7] though in these cases the study may present additional complications. One of them is evidently the inherent more complex synthesis of compounds with such characteristics, what have determined that the available information is less than that for homometallic compounds. A second issue to be taken into account is that the interacting magnetic centers may have different relaxation times T_1 or relaxation rates ($\nu = 1/T_1$). Briefly, T_1, which is very temperature dependent, measures the characteristic time for recovery of the magnetization of the paramagnetic system along the applied magnetic field direction after equilibrium has been disturbed. This fact makes it more difficult their study because one has to consider, in addition to all the temperature independent metal–metal interactions, the fact that the relaxation properties of the slowly relaxing center are influenced by the faster one.[5a,8] An additional approach to study interactions between paramagnetic centers with different relaxations rates, unfortunately less both employed and known, consists in doping a lattice of fast relaxing spin centers with a slowly relaxing paramagnetic impurity. This provides an interesting methodology to study by EPR interactions between distinct metal centers.[9] For those systems containing magnetic centers formed by two interacting $S = 1/2$ spins with different relaxation rates, the EPR resonance line associated with each center may be split by very weak spin-spin couplings such as isotropic exchange and dipole–dipole interaction. If one analyzes the EPR spectrum splitting of the slowly relaxing center at high temperature, no splitting is observed as one would expect for two interacting slowly relaxing centers. The situation is similar to that observed in the well-known chemical exchange phenomenon between two distinct chemical species showing different EPR resonance line positions that reversibly interconvert one to another with a characteristic jumping frequency. The resonance lines of the two species coalesce into one when the jumping frequency is higher than the line separation, but not when it is lower than the line separation. Similar arguments can be used in the above described case, with the only difference being that the jumping frequency is related to the relaxation rate ($1/T_1$) of the fast relaxing center. As a result, the fast relaxing center modulates the EPR signal splitting of the slowly relaxing one in such a way that at high temperature no splitting is observed because of the short value of T_1. At low temperature, the splitting is observed because of the longer value of T_1. This phenomenon may be theoretically interpreted using the Bloch–Wangsness–Redfield (BWR) theory or generalized Bloch equations.[5a,8a,8b,9e,10] In contrast, for a slowly relaxing paramagnetic center hosted in a lattice of fast relaxing spin centers, the analysis of the magnetic properties can be carried out in a similar way to that of a system presenting extended interactions,[3a–3c] though with some differences, as one has to take into account also the influence of the fast relaxing center on the magnetic properties of the slowly relaxing one.[9a,9b,9d,11]

In this paper we analyze the application of the previously discussed phenomena through the study of the magnetic properties of the pure *trans*-diaqua-bis(picolinato-*N*,*O*)-cobalt(II) dihydrate (**1**) and the corresponding Cu^{II} ion doped compound (**2**). Co^{II} and Cu^{II} ions are two transition metal ions showing different relaxation rates, with $\nu_{Co}{}^{II} >> \nu_{Cu}{}^{II}$. Magnetic and powder and single crystal EPR measurements of **1** and **2** together with computational calculations are used to evaluate the nature of the Co^{II}–Co^{II} and Cu^{II}–Co^{II} interactions as well as to predict the molecular structure of the copper impurity in **2**. These studies are complemented with powder and single crystal EPR measurements performed on Cu^{II}-doped *trans*-diaqua-bis-(picolinato-*N*,*O*)-zinc(II) dihydrate (**3**), with the pure Zn^{II} compound (**4**) being isomorphous to **1**.[12] The dependence with temperature of the Cu^{II} EPR resonance lines of **2** induced by the fast relaxing Co^{II} ion host as well as the evaluation of the Co^{II}–Cu^{II} isotropic exchange interaction are performed on the basis of the Anderson's theory of motional narrowing.[13] The role of the slowly relaxing Cu^{II} impurity in interrupting the Co^{II}–Co^{II} exchange interaction is also analyzed. This paper summarizes the different experimental methodologies using EPR complemented with magnetic measurements and computational calculations as required to get a full characterization of the magnetic properties of solid state compounds.

Results and Discussion

Crystal and Molecular Structure

A brief description of the crystal structure of **1** is presented in order to interpret the magnetic data and the EPR experiment.[12b] **1** crystallizes in the monoclinic system $P2_1/n$, $Z = 2$. The two symmetry related Co^{II} ion sites of the unit cell are designated as A (x, y, z) and B ($1/2 - x$, $1/2 + y$, $1/2 - z$). Co^{II} ions are in a slightly distorted octahedral environment coordinated to two water oxygen atoms (O2 and O2B), two carboxylic oxygen atoms (O1 and O1B) and two pyridine nitrogen atoms (N1 and N1B) of picolinic acid moieties (Figure 1).

Figure 1. Coordination around the Co^{II} ions of **1** with the Co-ligand distances in Å.

Co_A or Co_B sites are linked by symmetrical double hydrogen bond bridges each with topology –Co–O_2···O_1–Co- (d_{Co-Co}, 5.130 Å), which gives rise to Co^{II} ion chains running along the b crystal axis (see Figure 2). These two Co^{II} chains, which are symmetry related by the monoclinic C_2 rotation around the b axis, are held together by hydrogen bond interactions mediated by hydration water molecules. The shortest Co_A–Co_B distance is 9.096 Å. The structure of the Cu^{II} site in **2** and **3** will be inferred from the EPR and computational calculations below.

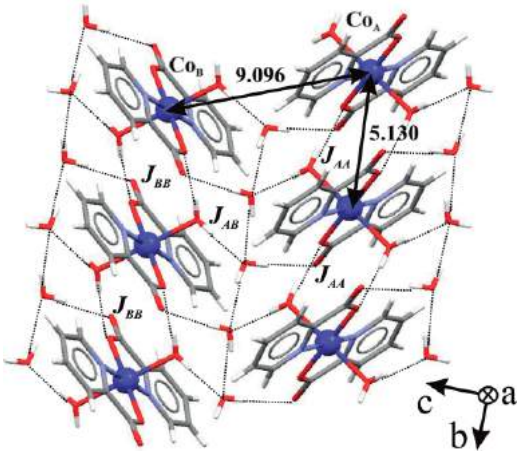

Figure 2. Crystal lattice perspective showing the hydrogen bond network (dotted lines) that links the symmetry related Co^{II} ions of **1**. Co_A stands for Co^{II} ions at the general position (*x*, *y*, *z*) whereas those labeled Co_B at (1/2 – *x*, 1/2 + *y*, 1/2 – *z*). Co^{II}–Co^{II} distances in Å are indicated as black double arrows. Chemical pathways bridging Co^{II} ions are labeled with the associated exchange coupling constants *J*.

Magnetic Data of 1

Temperature-dependent magnetic susceptibility (χ) and field-dependent magnetization (*M*) results are shown in Figure 3. Magnetization data were analyzed assuming Co^{II} ions in a high-spin configuration ($S = 3/2$) with a spin Hamiltonian that included the Zeeman interaction, and axial (*D*) and rhombic (*E*) zero field splitting parameters

$$\mathrm{H} = \mu_B \mathbf{S}\cdot\mathbf{g}\cdot\mathbf{B} + D\left(\mathbf{S}_z^2 - \frac{S(S+1)}{3}\right) + E\left(\mathbf{S}_x^2 - \mathbf{S}_y^2\right) \quad (1)$$

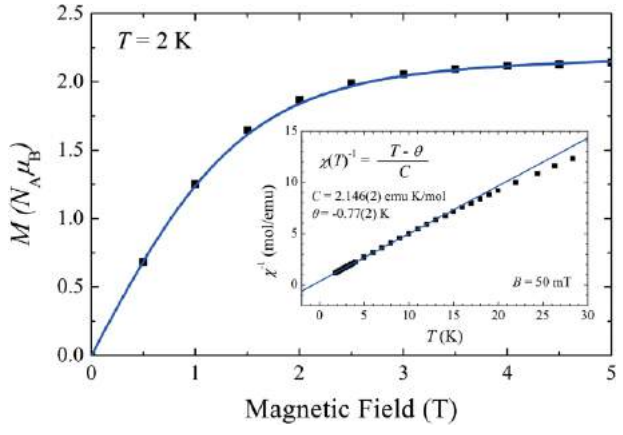

Figure 3. Molar magnetization *M* in $N_A\mu_B$ units as a function of magnetic field at 2 K of a powder sample of **1**. The solid line was obtained by least-squares fitting Equation 1 to the data. The inset shows the inverse of the molar magnetic susceptibility vs. temperature. The solid line in the inset was obtained by least-squares fitting a Curie–Weiss model to the data in the range of 2–12 K.

where all the symbols have the usual meaning and the sum over all Co^{II} sites of the crystal is omitted for simplicity.

A fitting procedure of the magnetization data yielded g_{iso} = 2.419(4) and D = 68.0(1) cm^{-1}, indicating that the ground doublet state corresponds to $M_S = \pm 1/2$. Inclusion of rhombic distortion and isotropic exchange interaction within the molecular field approximation, as implemented in the PHI program (see Exp. Sect.), did not show any improvement of the fitting. ZFS parameters and g_{iso} for the $S = 3/2$ multiplet are in line with Co^{II} ions in a pseudo octahedral coordination showing an orbital singlet ground state ($^4A_{2g}$) in which the two doublets of the original ^4F state of the free Co^{II} ion ($M_S = \pm 1/2$ and $M_S = \pm 3/2$) are split by spin-orbit coupling with excited states. The axial symmetry found for ZFS indicates that these split doublets may be considered pure in character. This compound was also previously studied by other authors, who found D = 84.24 cm^{-1}, E = 2.34 cm^{-1} and zJ = –0.05 cm^{-1}.[14] The discrepancies are likely due to the fact that these authors considered an anisotropic g-factor.

The large gap between $M_S = \pm 1/2$ and $M_S = \pm 3/2$ states ($2D$ = 136 cm^{-1}) reveals that the susceptibility data are not sensitive enough to obtain reliable ZFS parameters in the whole temperature range. For that reason, we analyzed the susceptibility data solely in the low temperature region (2–12 K, see inset on Figure 3), where only the lowest Kramers doublet ($M_S = \pm 1/2$) is thermally populated. This analysis, which was performed using a Curie–Weiss model assuming an effective spin $S' = 1/2$, yielded C = 2.146(2) emu K/mol and θ = –0.77(2) K. From the Curie constant value, we obtained g'_{iso} = 4.784(1), compatible for a high spin Co^{II} ion in an octahedral environment.[15] The θ value reveals very weak antiferromagnetic interaction between Co^{II} ions, which allowed us to estimate under the molecular field approximation $zJ_{1/2}$ = –2.14(2) cm^{-1}, where $J_{1/2}$ is the isotropic exchange interaction between $S' = 1/2$ effective spins.

EPR Measurements

Powder EPR spectra of **1** at different temperatures are shown in Figure 4, panel A. **1** presents an intense broad resonance at ca. 150 mT with no resolved hyperfine structure and peak to peak linewidth of ca. 60 mT at 4 K. This signal can be detected without significant changes on increasing temperature up to ca. 90 K, after which it broadens due to relaxation effects up to no detection. This spectrum is typical of high spin Co^{II} ions (S = 3/2) in octahedral coordination with ZFS > 0, in which the detected EPR transition occurs only within the ground doublet ($M_S = \pm 1/2$).[15a,16] The lack of hyperfine structure with the cobalt nucleus (I = 7/2, typically Co^{II} ions in octahedral environments present hyperfine parameters in the range of 20–180 × 10^{-4} cm^{-1})[15b,17] suggests that the weak exchange interaction detected by magnetic data is strong enough to collapse such a structure, which will be further analysed below from the single crystal EPR experiment.

Figure 4, panel B, shows two representative single crystal EPR spectra for two different magnetic field orientations indicated in the caption to the Figure. One or two single nearly Lorentzian shaped resonance lines depending on the magnetic field orientation are observed, in line with the monoclinic nature of the system. Since a broad single resonance line in the EPR experiment can be produced by anisotropic dipole–dipole interactions (anisotropic and antisymmetric exchange are usually ne-

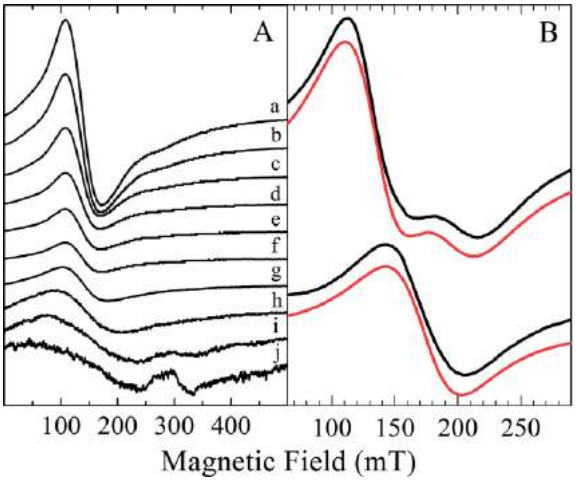

Figure 4. A) X-band powder EPR spectra of **1** at 4 K (a), 10 K (b), 20 K (c), 30 K (d), 40 K (e), 50 K (f), 70 K (g), 90 K (h), 110 K (i), and 130 K (j) under non-saturating conditions. The small signal at ca. 300 mT is a cavity background. B) Representative single crystal EPR spectra (black lines) obtained in the *ab* crystal plane at 10 K with the magnetic field at 15 degrees from the *a* crystal axis (upper) and in the *c*a* crystal plane at 165 degrees from the *c** axis (lower). Least squares simulations to the experimental spectra assuming two (upper) and one (lower) Lorentzian lineshapes are shown as red lines.

glected for very weak exchange coupled systems),[18] we evaluated the linewidth predicted by such interaction considering that it is solely determined by dipole–dipole interaction under the point dipole approximation for a 3D system (Figure S1). This calculation predicted linewidths in the range of 230–250 mT in the absence of exchange interactions in the *c*a* crystal plane, i.e. ca. 5 times larger than that observed in the EPR experiment (43–65 mT). This fact, together with the nearly Lorentzian lineshape of the EPR resonance lines, suggest the presence of exchange interactions that yield narrowing rather than broadening.[3a,15]

The Co^{II} g′-Matrix Evaluated from Single Crystal EPR Measurements

Since at low temperature only the lowest $M_S = \pm 1/2$ Kramers doublet is thermally populated, the system can be analysed assuming an effective $S' = 1/2$ spin

$$\mathbf{H}=\mu_B \mathbf{S'}_A \cdot \mathbf{g'}_A \cdot \mathbf{B} + \mu_B \mathbf{S'}_B \cdot \mathbf{g'}_B \cdot \mathbf{B} \quad (2)$$

where **g**′ are the **g**-matrices associated with each magnetically inequivalent Co^{II} ion, which contain information on the spin-orbit interaction and ZFS, and the sum over all the unit cells of the crystal lattice is omitted for simplicity. Since **1** crystallizes in a monoclinic space group, one should observe single crystal EPR spectra consisting of eight hyperfine components ($I = 7/2$) for any magnetic field orientation in the *c*a* plane and along the *b* axis, where Co_A^{II} and Co_B^{II} ions are magnetically equivalent, and two eight-line hyperfine spectra each associated with the two inequivalent Co^{II} ions for any other magnetic field direction. This situation was not observed in the spectral angular variation of **1**, which showed two partially overlapped single resonance lines in the *ab* and *c*b* crystal planes for most magnetic field orientations, and one single line in the *c*a* plane (representative EPR spectra are shown in Figure 4, panel B; the full angular variation of the spectra is shown as Supporting Information in Figure S2). Both the angular variation and the number of resonance lines are in line with the monoclinic nature of **1**, but the lack of a resolvable hyperfine pattern, as also observed in the powder EPR spectra, suggests the presence of isotropic exchange interactions between Co^{II} ions, strong enough to collapse such a structure. Hence, the single crystal EPR spectra of **1** were analysed assuming that the two partially overlapped resonance lines correspond to the two magnetically inequivalent Co_A^{II} and Co_B^{II} ion sublattices (see Figure 2).

To analyze the data, single crystal EPR spectra of **1** were least-squares fitted to the sum of two Lorentzian derivative functions with the same intensity. The positions of each resonance line were used to obtain the angular variation of g'^2-factors (Figure 5).

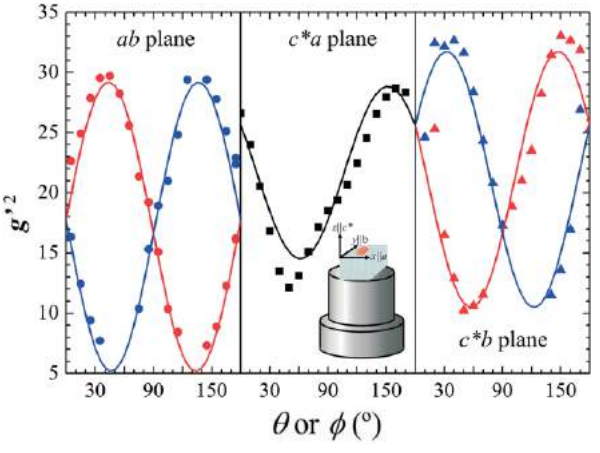

Figure 5. Angular variation of g'^2 for the two inequivalent Co^{II} sites in three crystal planes of **1**. Red and blue symbols identify the two magnetically inequivalent Co^{II} sites in the unit cell. In the *c*a* plane, both inequivalent Co^{II} ion sites are indistinguishable by EPR (black symbols). Solid lines were obtained by least-squares fitting the function **h**·**g**′·**g**′·**h**, where **h** is the magnetic field orientation, as explained elsewhere.[19] The inset shows the mounting and orientation of the single crystal of **1** for the EPR experiment. Some experimental points for two-line spectra are missed due to the large linewidth of one of the components, which precluded their precise position determination.

Least squares analysis of the g'^2 angular variation yielded the parameters given in Table 1, which were used to obtain the solid lines in Figure 5. As shown in this Figure there is a good agreement between our model and experimental data. The differences observed for some orientations are attributed to the uncertainties in the fitting of the resonance positions which arise from the large width of the EPR resonance lines. Because of the monoclinic symmetry of the crystal lattice of **1**, there are two possible assignments for the **g**′-matrix orientation in the molecular frame (Table 1 and Figure S3). As previously observed for low symmetry Co^{II} ions in high-spin configuration, the two possible orientations of the **g**′-matrix do not show any particular direction relative to the molecular frame.[15a] and references cited therein.

Table 1. g'^2-matrix and eigenvalues and eigenvectors of the two symmetry related Co^{II} ions of **1** in the experimental *abc** coordinate system. Upper and lower signs correspond to the two possible orientations due to the monoclinic nature of **1**.

g^2_{xx} = 17.7(4)	g^2_{xy} = ±12.0(6)
g^2_{yy} = 16.6(5)	g^2_{zx} = –6.0(5)
g^2_{zz} = 25.6(4)	g^2_{zy} = ∓9.6(5)
g_1 = 2.20(1)	$\boldsymbol{a}_1$ = [0.62(2), ∓0.76(1), –0.17(3)]
g_2 = 4.08(7)	$\boldsymbol{a}_2$ = [0.60(3), ±0.32(3), 0.74(1)]
g_3 = 6.22(5)	$\boldsymbol{a}_3$ = [0.51(1), ±0.56(1), –0.65(1)]

Exchange Interaction between Co^{II} Ions

We evaluated the isotropic exchange coupling constant by EPR on the basis of the Anderson's theory of motional narrowing.[13,20] Briefly, this theory predicts for a system consisting of two magnetically inequivalent paramagnetic centers with real or effective S = 1/2 spins, e.g. Co_A^{II} and Co_B^{II} ions of **1**, that the EPR resonances associated with each center coalesce into one resonance when $|J| > \mu_B \cdot \Delta g\ \bar{B}/2$•, where Δg and B are the difference between the g-factors and the gravity center of both resonances, respectively. This situation resembles that for two magnetically inequivalent chemical species that reversibly interconvert one to another with a characteristic exchange frequency, a phenomenon known as chemical exchange. Note that this model explains the collapse of the hyperfine structure of high spin Co^{II} ions into one line when |J| > A, where A is the hyperfine splitting.[21] As shown in Figure 5, for magnetic fields close to those directions where the two Co^{II} ion EPR signals associated with magnetically inequivalent cobalt sites tend to coalesce into one signal, i.e. close to the b, a, and c^* crystal axes, no detectable merging of the resonance lines corresponding to inequivalent Co^{II} ions was observed. Least square fitting of the spectra taken close to the above mentioned magnetic field directions, allowed us to evaluate ΔB ca. 20 mT as the minimum resolution limit to detect the resonance lines associated with Co_A and Co_B species. This value was used to evaluate an upper limit for the isotropic exchange interaction between Co_A and Co_B using the Anderson's theory of exchange narrowing, which predicts $|J_{1/2}| < \mu_B \cdot \Delta g\ \bar{B}/2$ ca. 0.02 cm^{-1}, where the subscript 1/2 stands for the isotropic exchange constant between S' = 1/2 spins. This J value confirms that the exchange coupling, if present, is not significant enough to collapse the resonance lines corresponding to inequivalent Co^{II} ions. Hence, $zJ_{1/2}$ = –2.14(2) cm^{-1} determined by magnetic low temperature susceptibility measurements can mainly be ascribed to the exchange interaction between magnetically equivalent Co^{II} ions. Considering z = 2, this isotropic exchange interaction was evaluated to be $J_{1/2}$ = –1.07(1) $cm^{-1} \equiv J_{3/2}$ = –0.357(3) cm^{-1}, according to the relation $J_{1/2} = 3 \times J_{3/2}$ demonstrated elsewhere.[15b] This weak exchange interaction is mediated by symmetrical double hydrogen bonds between coordinated water molecules and carboxylate oxygen atoms from picolinic moieties coordinated to closest magnetically equivalent Co^{II} ions (Figure 2) and is responsible for merging the Co^{II} hyperfine structure, not detectable in the EPR experiment.

In line with experiment, computational calculations determined a high spin S = 3/2 ground spin state for the Co^{II} ions of **1**, with the 1/2 low spin state being separated by more than 1×10^4 cm^{-1}. Thus, in all the models the Co atoms were computed with a S = 3/2 spin state. The electron spin density is mainly located on the Co^{II} ion (2.83), whereas 0.17 is delocalized on the ligands. To rationalize the experimentally determined J values in **1** with those obtained by computational calculations, different models based on the crystallographic structure were built.[12b] For $J_{3/2}^{AA}$, three models containing two, three, and five consecutive Co^{II} monomers were built, while for $J_{3/2}^{AB}$ a single model containing two adjacent monomers of one chain and two of the closest neighboring chain was used. Calculations using the different models yielded very similar energy gaps E_{AF}–$E_F \approx J_{3/2}^{AA} = J_{3/2}^{BB}$ ca. – 0.24 cm^{-1}, indicating that magnetically equivalent Co^{II} ions belonging to a chain are antiferromagnetically coupled in good agreement with experiment. No significant $J_{3/2}^{AB}$ was detected, i.e. it fell into the detection limit of the energies calculated with this computational method (see Exp. Sect.).

Powder and Single Crystal EPR Measurements of 2

Cu^{II} and Co^{II} ions are, as said above, two Kramers ions with different relaxation rates ($\nu_{Co}^{II} >> \nu_{Cu}^{II}$), which may produce temperature-dependent modifications of the spectra of the slowly relaxing Cu^{II} ion when they are coupled.[5a,8b,9,10] A powder sample of **2** showed at high temperature a nearly axial Cu^{II} EPR spectrum with resolved hyperfine structure with the copper nucleus (I = 3/2) at $g_{||}$ (Figure 6, panel A, spectrum i) and no distinguishable resonance lines associated with Co^{II} ions. On decreasing temperature, the Cu^{II} resonance lines broaden, with no shift in position, in line with the decreasing Co^{II} relaxation rate. This temperature behavior of the Cu^{II} EPR spectra indicates

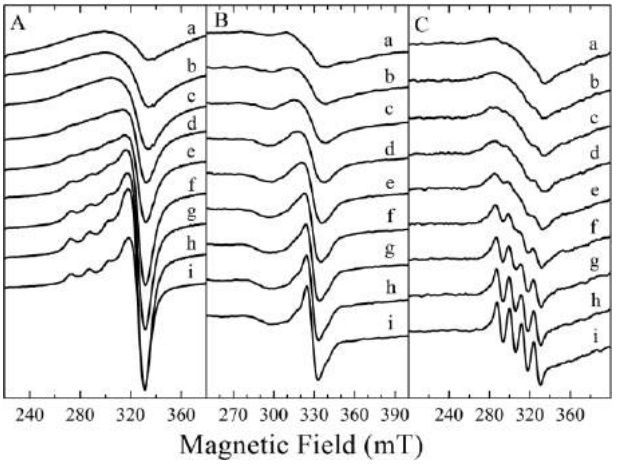

Figure 6. Panel A. Powder X-band EPR spectra of **2** as a function of temperature, a) 140 K, b) 160 K, c) 180 K, d) 200 K, e) 220 K, f) 240 K, g) 260 K, h) 280 K, and i) 300 K under non-saturating conditions. Panels B and C, idem A but for single crystal EPR spectra in the c^*a crystal plane for two magnetic field orientations (panel B and panel C, 100 degrees and 170 degrees from the c^* crystal axis, respectively). Spectra were taken under the same experimental conditions. No significant changes in lineshape are observed above 300 K.

that the main Cu^{II}–Co^{II} interactions produce broadening rather than narrowing of the Cu^{II} resonances. A similar conclusion can be obtained from EPR studies performed on single crystals of **2** (Figure 6, panels B and C), which showed very broad Cu^{II} EPR resonance lines at low temperature but the typical four hyperfine pattern at high temperature. Hence, as stated in the introduction, the broadening of the Cu^{II} ion resonance lines when decreasing temperature is due to Cu^{II}–Co^{II} dipolar interactions which are averaged out at high temperature, but not at low temperature where the relaxation rate of the Co^{II} ion is low.

The temperature behavior of Cu^{II} EPR spectra of **2** can be interpreted with the random frequency modulation model proposed by Anderson.[20] This model assumes that the Hamiltonian describing the system may be split up into three parts

$$H = H_o + H_p + H_m \quad (3)$$

where H_o, the unperturbed Hamiltonian (Zeeman + hyperfine terms), determines the position of the resonance line(s); H_p, the perturbing Hamiltonian, which does not commute either with H_o or with H_m, is determined by the dipolar interaction and eventually anisotropic exchange interactions; H_m, the motional Hamiltonian, that commutes with H_o but not with H_p, cannot change the position of the resonance lines determined by H_o but can cause the time dependence of H_p, which determines the lineshape of the resonance lines.[13,20]

In the classical exchange narrowing case, H_m is given by the temperature independent isotropic exchange interaction ($H_{me} = \omega_{ex}\, \mathbf{S}_{Cu}\cdot\mathbf{S}_{Co}$, where $\omega_{ex} \approx J/\hbar$), whereas in the host spin lattice relaxation narrowing case, H_m is determined by the temperature dependent spin lattice relaxation parameter T_1 of the Co^{II} host ion.[11a] For the case we are analyzing here, it is evident that the main contribution to H_m is determined by the host spin lattice relaxation rate as the changes in linewidth of the Cu^{II} resonance lines are highly temperature dependent, but, as we will see below, the contribution of the isotropic exchange interaction shows, though small, non-negligible contributions to the total Hamiltonian H, which is also reflected in the EPR spectra. The fact that H_m is determined by two distinct contributions suggests that their discrimination, particularly when $H_{msl} >> H_{me}$, could be difficult as both simultaneously determine the time dependence of H_p and hence the lineshape of the EPR spectra. However, this apparent disadvantage for the less intense interaction (H_{me}) can be used to evaluate the effect of both Hamiltonians by analyzing the effect of H_{me} on both position and width of the EPR resonance line at high temperature, as the broadening effect of H_p is averaged out by H_{msl}. In other words, the analysis of the single crystal Cu^{II} EPR spectra at high temperature can be used to evaluate the exchange coupling constant J between Co^{II} and Cu^{II} spins, which will be seen below.

g-Matrix of the Cu^{II} Impurity of 2 and 3

To evaluate the Cu^{II} ion ***g***-matrix of **2**, we performed EPR measurements on oriented single crystals at room temperature for different magnetic field orientations. The angular variation of the Cu^{II} impurity EPR spectra corresponds to the expected one for a monoclinic system, i.e. two groups of four resonance lines each associated with magnetically inequivalent Cu^{II} ions in the *ab* and *c*b* planes, and only one in the *c*a* plane, in line with the angular variation observed for the Co^{II} ions of **1**. This fact indicates that some Co^{II} ions are substituted with Cu^{II} impurities in the crystal lattice of **1** to give **2**. Representative room temperature spectra obtained in the *c*a* plane are shown in Figure 6, panels B and C (spectra i) for two different magnetic field orientations. The full angular variation of the spectra in the three crystal planes is shown in Figure S4.

For some magnetic field orientations in the *c*a* plane, EPR spectra could be simulated assuming four Gaussian-shaped resonance lines, as expected for a Cu^{II}-doped magnetic system (see spectrum i in Figure 6, panel C). Spectral simulations in the *c*b* and *ab* planes were obtained assuming either two groups of four resonance lines when the resolution was large enough to detect resolved hyperfine interaction, or one group of four resonance lines plus one single resonance for other orientations (see Supporting Information for details, Figure S4). The gravity centers of the spectra thus determined were used to obtain the angular variation of the g^2-factors of the Cu^{II} impurity of **2** (Figure 7). The ***g***-matrix associated with the Cu^{II} impurity of **2** (Table 2) was obtained as explained for **1** (see above). As for **1**, there are two possible ***g***-matrix orientations (Figure S5 and Table 2). The inset on Figure 7 shows the assigned Cu^{II} ***g***-matrix relative to the molecular frame of the Co^{II} site in **1**, which is based on well-known magneto structural correlations established for Cu^{II} compounds. The fact that the highest g value is lying nearly along the Co–O2 bond confirms that the Jahn–Teller distortion suffered by the Cu^{II} site is along this direction.

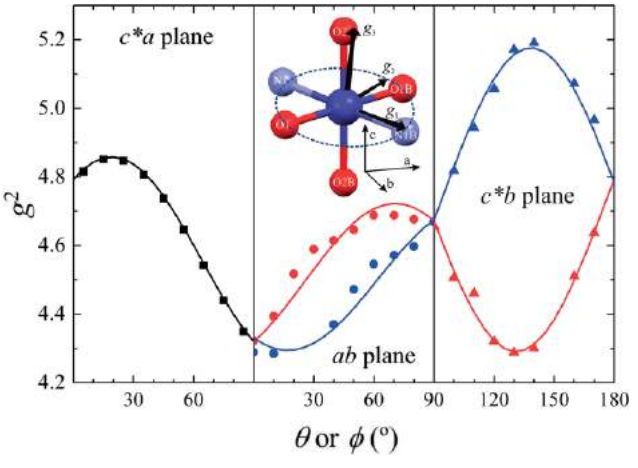

Figure 7. Angular variation of $g^2(\theta,\phi)$ for the two magnetically inequivalent Cu^{II} sites in three crystal planes of **2**. Red and blue colors identify each magnetically inequivalent Cu^{II} site in the *ab* and *c*b* crystal planes. Only one group of four resonance lines (black) is observed in the *c*a* plane indicating that Cu^{II} impurities follow the symmetry of the Co^{II} site in the pure compound **1**. Some experimental points are missed due to uncertainties in the spectral gravity center determination associated with inequivalent copper site. The inset shows the assigned orientation for the Cu^{II} ion ***g***-matrix in the Co^{II} site molecular frame.

The EPR experiment was also performed on an oriented single crystal of **3**, in which Cu^{II} impurities are hosted in a diamagnetic Zn^{II} lattice isomorphous to **1**. Eigenvalues and eigenvec-

Table 2. Components of the Cu^{II} $\mathbf{g}^2$-matrix of **2** and **3** together with eigenvalues and eigenvectors in the *xyz* = *abc** coordinate system.

2	
g^2_{xx} = 4.320 (6)	g^2_{xy} = ±0.142 (8)
g^2_{yy} = 4.673 (6)	g^2_{zx} = 0.187 (8)
g^2_{zz} = 4.794 (6)	g^2_{zy} = ±0.438 (7)
g_1 = 2.062(2)	$\boldsymbol{a}_1$ = [0.89(6), ±0.1(1), –0.43(9)]
g_2 = 2.073(2)	$\boldsymbol{a}_2$ = [0.4(2), ∓0.76(2), 0.53(7)]
g_3 = 2.288(2)	$\boldsymbol{a}_3$ = [0.248(7), ±0.633(4), 0.733(3)]
3	
g^2_{xx} = 4.319 (5)	g^2_{xy} = ±0.107 (6)
g^2_{yy} = 4.676 (5)	g^2_{zx} = 0.156 (6)
g^2_{zz} = 4.779 (5)	g^2_{zy} = ±0.437 (6)
g_1 = 2.064(2)	$\boldsymbol{a}_1$ = [0.75(7), 0.38(7), ∓0.54(4)]
g_2 = 2.075(2)	$\boldsymbol{a}_2$ = [0.63(8), –0.66(4), ±0.41(6)]
g_3 = 2.282(2)	$\boldsymbol{a}_3$ = [0.207(6), ±0.646(3), 0.735(3)]

tors are very similar to those obtained in **2** (Table 2), indicating that Cu^{II} impurities can substitute for both Co^{II} or Zn^{II} ions suffering the same Jahn–Teller distortion, independently of the host matrix (Figure S5). The only difference observed resides in the larger linewidth of the individual Cu^{II} resonance lines in **2**, confirming that these changes are due to the magnetic nature of the host lattice. This observation will be discussed below.

To confirm the EPR conclusion regarding that the Cu^{II} site Jahn–Teller distortion is along the Cu-O2 bond, we evaluated the structure of the Cu^{II} impurity in **2** by computational calculations. After relaxation of the copper monomer keeping fixed the crystal structure of **1**, some small changes were observed for the Cu^{II} site relative to the geometry of the Co^{II} site. The atomic coordinates of the calculated structures are given in the Supporting Information (Table S1). The main difference is that both Cu–N1 (d_{Cu-N1} = 1.999 Å) and Cu–O1 (d_{Cu-O1} = 1.965 Å) distances decreased compared to those of the Co^{II} compound

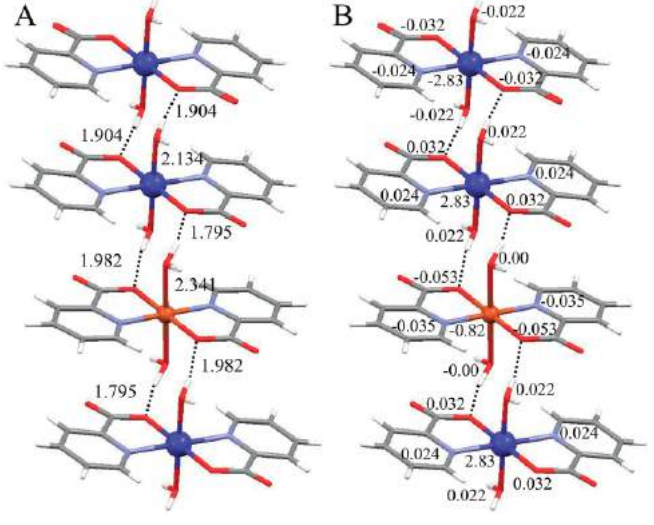

Figure 8. Panel A and B show a Co^{II} ion chain interrupted by a Cu^{II} ion impurity. The hydrogen bonds bridging the metal centers are indicated with dotted lines. Relevant bond lengths in Å are given in panel A, whereas spin densities are given in panel B.

(see Figure 1). The Cu–O2 distances (d_{Cu-O2} = 2.341 Å) increased to form an axially elongated octahedron, in line with the EPR results (Figure S5). Despite the elongation of the Cu-O2 distance, the hydrogen bond interactions with the surrounding water molecules are conserved (Figure 8, panel A). Results obtained by both EPR and calculations, are expectable considering the lower energetic cost that implies the displacement of water molecules relative to the picolinic acid molecules (see Figure 1 and Figure 2).

Cu^{II}–Co^{II} Exchange Interactions

Results shown in Figure 6 indicate that the EPR spectra broadening observed in **2** at low temperature are averaged out at high temperature because of the higher relaxation rate of the Co^{II} ions relative to that of the Cu^{II} ions. These temperature dependent changes in linewidth were not observed in **3**, indicating the magnetic origin of the broadening in **2**. No significant narrowing is detected above 300 K in **2**, indicating that dipolar interaction are totally averaged to zero at high temperature. The lowering of the hyperfine linewidth with increasing temperatures observed in **2** occurs when the broadening interactions can be described through matrices with a trace of zero, as is the case of the dipolar interaction, but not for isotropic exchange. The fact that single crystal Cu^{II} EPR spectra of **2** show resolved hyperfine structure for most magnetic field orientations, indicates that the magnitude of the Cu^{II}–Co^{II} isotropic exchange is very weak to collapse the hyperfine structure and much lower than the Cu^{II}–Co^{II} dipolar interactions. A comparison between the EPR spectra of **2** and **3** for those magnetic field orientations showing well-resolved four hyperfine components reveals spectra having approximately the same position and hyperfine splitting but with the hyperfine linewidths for **2** being larger than for **3**. This difference is undoubtedly attributed to the isotropic exchange interaction which is operative in **2** (Cu^{II} ions embedded in a paramagnetic matrix) but not in **3** (Cu^{II} ions embedded in a diamagnetic matrix). Note that the Anderson model predicts for a weak exchange regime ($|J| < A$) a broadening ($\Gamma + \omega_{ex}$) of the individual hyperfine lines, where Γ is the intrinsic linewidth of each hyperfine component of the Cu^{II} ion EPR spectra in the absence of exchange.[21] With this in mind, we simulated the experimental EPR spectra of **2** using Anderson arguments for a situation of weak exchange regime. The employed procedure is explained elsewhere.[21] Figure 9, panel A shows a representative spectrum for a given magnetic field orientation where the hyperfine splitting is maximal, together with simulations using the Anderson's model with increasing exchange frequency values. This procedure allowed us to determine ω_{ex} = 90 MHz = 0.003 cm^{-1}. Panel B shows the experimental spectral angular variation for the *c**a* crystal plane together with simulation using that exchange frequency value. As revealed in the Figure simulations are in a very good agreement with the experimental spectra, which evidence the robustness of the method.

The Cu^{II}–Co^{II} exchange interaction was also evaluated by computational calculations using two, three, and five consecutive monomers models containing a copper atom in sequences

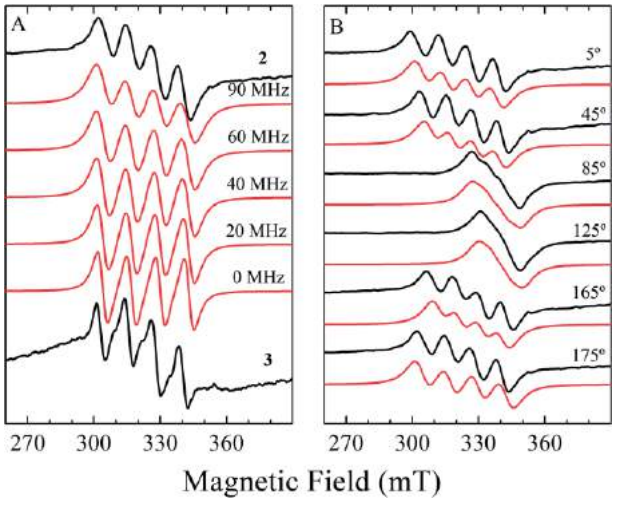

Figure 9. Panel A shows simulation of the experimental EPR spectrum of **2** taken at 175 degrees from the *c** axis (black line, **2**) as a function of increasing exchange frequencies (red lines) using Anderson's model for a weak exchange regime ($\hbar\omega_{ex} << A$, where A is the hyperfine splitting). The linewidths used in simulation were obtained from a spectrum of **3** taken under the same experimental condition (bottom of panel A, black line, **3**). Panel B shows the angular variation of the EPR spectra of **2** (black line) in the *c***a* crystal plane together with simulation (red line) using ω_{ex} = 90 MHz (see text).

such as Cu–Co, Co–Cu–Co, and Co–Co–Cu–Co–Co. Calculations yielded an antiferromagnetic ground state with $J_{Cu^{II}-Co^{II}} \approx -0.02$ cm^{-1}, an order of magnitude smaller than that for Co^{II}–Co^{II} ($J_{3/2}^{AA} = J_{3/2}^{BB} = -0.24$ cm^{-1}), in line with the experimentally determined value by EPR ($|J| = 0.0015$ cm^{-1}). Both experiment and computational calculations indicate that the infinite chains of coupled Co^{II} ions are converted to independent fragments of coupled Co^{II} ions upon copper doping. The Cu-ligand distances as well as the spin density on the Cu^{II} ion and its ligands are shown in Figure 8.

The above results indicate that incorporating a magnetic ion like Cu^{II} in an infinite chain of Co^{II} ions interrupts the exchange interaction transmitted by the double hydrogen bonds bridging Co^{II} ion pairs present in **1**. One can wonder what causes the decrease of the Cu^{II}–Co^{II} exchange interaction relative to the Co^{II}–Co^{II} one as the bridging topology is relatively similar. This fact can be ascribed to two factors. One of them is evidently determined by the Jahn–Teller distortion suffered by the incorporated Cu^{II} ions, which led to a decreasing spin density at the apical copper O2 ligands (see Figure 8, panel B). The second one is related to the absence of symmetry in the Cu^{II}–Co^{II} double hydrogen bond (Figure 8). It has theoretically been analyzed that the condition for maximum isotropic exchange coupling is related to a pathway presenting a generalized reflection-inversion symmetry, as is the case for **1** (Figure 2, see J_{AA} or J_{BB}).[22] This symmetry is lost in **2**, which implies that the two different hydrogen bonds bridging Cu^{II} and Co^{II} ions interfere destructively.

Conclusions

In this work we study the magnetic properties of a pure cobalt compound and how a slowly relaxing Cu^{II} impurity interrupts the Co^{II}–Co^{II} exchange interaction. Co^{II} ions are in high-spin configuration, forming structural chains in which the metal centers are bridged by symmetrical double hydrogen bonds. Magnetic measurements, EPR spectroscopy, and computational calculations demonstrated that this chemical pathway transmits very weak antiferromagnetic exchange interactions ($J_{1/2}$ = –1.07 cm^{-1}). When this compound is doped with Cu^{II} ions, the structural Co^{II} chains are interrupted by the presence of the impurity. Single crystal EPR performed on the copper-doped compound revealed the presence of very weak Cu^{II}–Co^{II} exchange interactions ($|J| = 0.0015$ cm^{-1}). This doping procedure gives rise to segmented structures of Co^{II} ion oligomers, which can be considered as magnetic blocks formed by a finite number of Co^{II} ions coupled by exchange. The experimental work was complemented with computational calculations that confirmed the structural changes experienced by the chemical pathways bridging the metal centers when doped with a copper impurity. The loss of symmetry of the superexchange chemical pathway is the principal reason for the lower value of the exchange coupling constant between copper and cobalt. This work shows that EPR can advantageously be used to evaluate weak exchange interactions between metal centers with different relaxation rates by using the fact that those metal–metal interactions that broaden the EPR resonance line (e.g. dipolar interaction) and that are described by matrices with a trace of zero are averaged out at high temperatures.

Experimental Section

Materials: All chemicals, of commercially available reagent grade, were used as received.

1 and 4: Compounds were prepared in a different way to those reported elsewhere.[12b,12a] $Co(CH_3COO)_2{\cdot}4H_2O$ or $Zn(CH_3COO)_2{\cdot}2H_2O$ (1 mmol, 0.249/0.219 g, Avocado Research Chemicals/Merck, respectively), and picolinic acid (2 mmol, 0.246 g, Sigma–Aldrich) were dissolved in 50 mL of deionized water. Solutions were filtered using a 0.22 μm Millipore cellulose nitrate membrane and left to evaporate slowly at room temperature. After a few days orange-colored prismatic single crystals of **1** and colourless single crystals of **4** were obtained. They were filtered, washed with a small amount of cold water, and dried under air. Yield (crystals): 45 %. Elemental analyses (C, H, N) were performed on a LECO® CHN628 Series Elemental Determinator. Calcd for **1**/**4** ($C_{12}H_{16}N_2O_8Co_1/Zn_1$): C, 38.4; H, 4.3; N, 7.5; found for **1**/**4** C, 38.0/37.5; H, 4.4/4.2; N, 7.5/7.4.

2 and 3: The Cu^{II}-doped Co^{II} and Zn^{II} analogues were prepared by adding a solution containing $Cu(CH_3COO)_2{\cdot}H_2O$ (2 mM) plus picolinic acid (4 mM) to a solution of **1** and **4**, respectively, in 1:10 Cu:Co/Zn ratios. Pale orange (**2**) and pale light blue (**3**) single crystals with the same external morphology to **1** and **4**, respectively, were obtained after a few days. Powder samples of **1**, **2**, **3**, and **4** were obtained by grinding single crystals. Metal analysis were performed by atomic absorption spectrometry on a Perkin–Elmer PinAAcle 900 T spectrometer. Found 0.71 Cu/10 Co and 0.89 Cu/10 Zn for **2** and **3**, respectively.

Powder X-ray and Morphology of the Single Crystals: Structures of **1** and **4** were confirmed from powder X-ray diffraction data taken on a Shimadzu XD-D1 diffractometer, and correspond to those previously reported.[12b,12a] Powder X-ray diffractograms for all compounds are shown in Figure S6. The morphology of single crystals

of **1**, **2**, **3**, and **4** were determined by measuring the angles between crystal faces using a Carl Zeiss Axiolab goniometric microscope. Single crystals showed well developed (001) faces.

Magnetic Measurements: Magnetic data were obtained with a Quantum Design MPMS2 SQUID magnetometer. Magnetization and magnetic susceptibility measurements were performed on 42 mg of a powder sample of **1** encapsulated on a gelatin container of known diamagnetic contribution as a function of the external DC magnetic field (between 0 and 5 T) at 2 K and as a function of temperature (between 2 and 300 K) at 50 mT, respectively. The molar magnetic susceptibility values were corrected for diamagnetism ($\chi_{DIA} = -143 \times 10^{-6}$ cm^3 mol^{-1}) using the Pascal's constants.[23] The fitting procedure of the magnetic data was performed using the PHI software.[24]

EPR Measurements: Variable temperature X-band CW-EPR measurements were performed on a Bruker EMX-Plus spectrometer, equipped either with a nitrogen continuous-flow cryostat (100–340 K) or with an Oxford helium continuous-flow cryostat (4–100 K) and a rectangular cavity with 100 kHz field modulation. X-band CW-EPR spectra of oriented single crystals of **1** were obtained at 10 K, whereas those of **2** and **3** in the range 100 K–340 K.

Single crystals of **1**, **2**, and **3** were oriented by gluing their (001) faces to a cleaved KCl cubic holder, which defined a set of orthogonal laboratory axes with the *y* direction corresponding to the crystal *b* axis, a fact confirmed by the symmetry of the angular variation of the EPR signals in the *xy* and *zy* planes. The cubic sample holder was placed on the top of a Rexolite cylinder which was fitted to the end of a 4 mm OD quartz tube, as explained elsewhere.[19] The tube was positioned at the center of the microwave cavity and attached to a goniometer which allowed the sample to be rotated with the magnetic field in the *xy*, *zx*, and *zy* ($y \| b$ and $x \| a$) planes of **1**, **2**, and **3** (see inset on Figure 5).

Computational Calculations: The first-principle screened exchange hybrid density functional of Heyd, Scuseria, and Ernzerhof (HSE) with the basis set 6-311G (d,p) was used to compute the energy of the antiferromagnetic (AFM) and the ferromagnetic (FM) states as implemented in GAUSSIAN suite of programs.[25] HSE functional was successfully used to predict the correct spin localization and the magnetic state of other systems.[26] The exchange coupling *J* is proportional to the difference in energy of the AFM and FM states. In order to build the AFM and FM states we used the fragment procedure implemented in GAUSSIAN.[25c]

The SCF convergence was achieved up to 10^{-9} Hartree (2×10^{-4} cm^{-1}). Calculations were based on the crystallographic structures of **1** and **4**, which includes the heavy atoms and also the hydrogen atoms. No structural relaxation was allowed.

Acknowledgments

We thank FONCyT, CONICET, and CAI+D-UNL for financial support. A. L. P. thanks CONICET for a fellowship grant. S. D. D and C. D. B. are members of CONICET-Argentina.

Keywords: Cobalt. Copper. EPR spectroscopy. Exchange interactions. Magnetic properties

[1] a) M. Cortijo, V. Bulicanu, K. S. Pedersen, M. Rouzières, J. Bendix, R. Clérac, E. A. Hillard, *Eur. J. Inorg. Chem.* **2018**, 320–325; b) S. L. Lambert, D. N. Hendrickson, *Inorg. Chem.* **1979**, *18*, 2683–2686; c) D. Gatteschi, *Adv. Mater.* **1994**, *6*, 635–645; d) J. P. S. Walsh, S. Sproules, N. F. Chilton, A.-L. Barra, G. A. Timco, D. Collison, E. J. L. McInnes, R. E. P. Winpenny, *Inorg. Chem.* **2014**, *53*, 8464–8472; e) M. L. Kirk, D. A. Shultz, D. E. Stasiw, D. Habel-Rodriguez, B. Stein, P. D. Boyle, *J. Am. Chem. Soc.* **2013**, *135*, 14713–14725; f) M. V. Fedin, S. L. Veber, E. G. Bagryanskaya, V. I. Ovcharenko, *Coord. Chem. Rev.* **2015**, *289–290*, 341–356; g) Y. Journaux, J. Ferrando-Soria, E. Pardo, R. Ruiz-Garcia, M. Julve, F. Lloret, J. Cano, Y. Li, L. Lisnard, P. Yu, H. Stumpf, C. L. M. Pereira, *Eur. J. Inorg. Chem.* **2018**, *2018*, 228–247; h) C. Mathonière, *Eur. J. Inorg. Chem.* **2018**, *2018*, 248–258; i) M. G. Alexandru, D. Visinescu, S. Shova, M. Andruh, F. Lloret, M. Julve, *Eur. J. Inorg. Chem.* **2018**, *2018*, 360–369; j) S. Ostrovsky, Z. Tomkowicz, W. Haase, *Coord. Chem. Rev.* **2009**, *253*, 2363–2375. ***((<=PM: CrossRef notyet done))***.

[2] a) V. Lloveras, E. Badetti, K. Wurst, V. Chechik, J. Veciana, J. Vidal-Gancedo, *Chem. Eur. J.* **2016**, *22*, 1805–1815; b) M. Jurić, D. Pajić, D. Žilić, B. Rakvin, K. Molčanov, J. Popović, *Dalton Trans.* **2015**, *44*, 20626–20635; c) R. A. Allao, A. K. Jordao, J. A. L. C. Resende, A. C. Cunha, V. F. Ferreira, M. A. Novak, C. Sangregorio, L. Sorace, M. G. F. Vaz, *Dalton Trans.* **2011**, *40*, 10843–10850; d) L. Sorace, C. Sangregorio, A. Figuerola, C. Benelli, D. Gatteschi, *Chem. Eur. J.* **2009**, *15*, 1377–1388.

[3] a) R. Calvo, *Appl. Magn. Reson.* **2007**, *31*, 271–299; b) S. K. Hoffmann, W. Hilczer, J. Goslar, *Appl. Magn. Reson.* **1994**, *7*, 289–321; c) A. C. Rizzi, N. I. Neuman, P. J. González, C. D. Brondino, *Eur. J. Inorg. Chem.* **2016**, 192–207; d) D. Žilić, D. Maity, M. Cetina, K. Molčanov, Z. Džolić, M. Herak, *ChemPhysChem* **2017**, *18*, 2397–2408; e) P. Gast, E. J. J. Groenen, in *eMagRes, Vol. 5*, **2016**, pp. 1435–1444; f) D. Maganas, S. Milikisyants, J. M. A. Rijnbeek, S. Sottini, N. Levesanos, P. Kyritsis, E. J. J. Groenen, *Inorg. Chem.* **2010**, *49*, 595–605; g) J. Titiš, R. Boča, *Inorg. Chem.* **2011**, *50*, 11838–11845; h) M. Idesicova, J. Titiš, J. Krzystek, R. BoÄýa, *Inorg. Chem.* **2013**, *52*, 9409–9417.

[4] a) N. I. Neuman, E. Burna, R. Baggio, M. C. G. Passeggi, A. C. Rizzi, C. D. Brondino, *Inorg. Chem. Front.* **2015**, *2*, 837–845; b) C. D. Brondino, N. M. C. Casado, M. C. G. Passeggi, R. Calvo, *Inorg. Chem.* **1993**, *32*, 2078–2084; c) C. A. Steren, R. Calvo, O. E. Piro, B. E. Rivero, *Inorg. Chem.* **1989**, *28*, 1933–1938; d) B. Natarajan, S. Mithira, S. Deepa, P. Sambasiva Rao, *Appl. Magn. Reson.* **2008**, *35*, 57–71; e) D. Srinivas, M. V. B. L. N. Swamy, S. Subramanian, *Mol. Phys.* **1986**, *57*, 55–63.

[5] a) C. More, M. Asso, G. Roger, B. Guigliarelli, J. Caldeira, J. Moura, P. Bertrand, *Biochemistry* **2005**, *44*, 11628–11635; b) C. D. Brondino, M. G. Rivas, M. J. Romao, J. J. Moura, I. Moura, *Acc. Chem. Res.* **2006**, *39*, 788–796; c) R. Calvo, M. C. Passeggi, R. A. Isaacson, M. Y. Okamura, G. Feher, *Biophys. J.* **1990**, *58*, 149–165; d) S. S. Eaton, G. R. Eaton, *Coord. Chem. Rev.* **1978**, *26*, 207–262.

[6] a) T. Gong, X. Yang, J. J. Fang, Q. Sui, F. G. Xi, E. Q. Gao, *ACS Appl. Mater. Interfaces* **2017**, *9*, 5503–5512; b) R. R. Baum, C. D. James, D. L. Tierney, in *Future Directions in Metalloprotein and Metalloenzyme Research* (Eds.: G. Hanson, L. Berliner), Springer International Publishing, Cham, pp. 33–54; c) K. E. Prosser, C. J. Walsby, *Eur. J. Inorg. Chem.* **2017**, *2017*, 1573–1585; d) W. R. Hagen, *Biomolecular EPR spectroscopy*, CRC press, Boca Raton, FL, **2008**; e) P. Maslewski, D. Wyrzykowski, M. Witwicki, A. Dołęga, *Eur. J. Inorg. Chem.* **2018**, *2018*, 1399–1408; f) Z. G. Lada, Y. Sanakis, C. P. Raptopoulou, V. Psycharis, S. P. Perlepes, G. Mitrikas, *Dalton Trans.* **2017**, *46*, 8458–8475; g) E. A. Suturina, J. Nehrkorn, J. M. Zadrozny, J. Liu, M. Atanasov, T. Weyhermüller, D. Maganas, S. Hill, A. Schnegg, E. Bill, J. R. Long, F. Neese, *Inorg. Chem.* **2017**, *56*, 3102–3118.

[7] a) Y. L. Qin, B. W. Yang, G. F. Wang, H. Sun, *Acta Crystallogr., Sect. C* **2016**, *72*, 555–560; b) A. C. Rizzi, R. Calvo, R. Baggio, M. T. Garland, O. Peña, M. Perec, *Inorg. Chem.* **2002**, *41*, 5609–5614; c) E. Coronado, M. Drillon, P. R. Nugteren, L. J. de Jongh, D. Beltran, *J. Am. Chem. Soc.* **1988**, *110*, 3907–3913; d) J. J. Borras-Almenar, E. Coronado, D. Gatteschi, C. Zanchini, *Inorg. Chem.* **1992**, *31*, 294–298.

[8] a) K. M. Salikhov, R. T. Galeev, V. K. Voronkova, Y. V. Yablokov, J. Legendziewicz, *Appl. Magn. Reson.* **1998**, *14*, 457–472; b) P. J. González, G. I. Barrera, A. C. Rizzi, J. J. G. Moura, M. C. G. Passeggi, C. D. Brondino, *J. Inorg. Biochem.* **2009**, *103*, 1342–1346; c) S. S. Eaton, G. R. Eaton, *Coord. Chem. Rev.* **1988**, *83*, 29–72.

[9] a) I. Yildirim, B. Karabulut, O. Büyükgüngör, *Spectrochim. Acta Part A* **2016**, *152*, 608–613; b) I. Ucar, B. Karabulut, A. Bulut, O. Büyükgüngör, *Spectrochim. Acta Part A* **2008**, *71*, 1239–1245; c) K. Velavan, R. Venkatesan, P. Sambasiva Rao, *Spectrochim. Acta Part A* **2005**, *62*, 494–499; d) R. M. Krishna, S. V. J. Lakshmana, *Radiat. Eff. Defects Solids* **1994**, *132*,

67–73; e) I. Sougandi, R. Venkatesan, P. S. Rao, *Spectrochim. Acta Part A* **2004**, *60*, 2653–2660.
[10] L. Fielding, K. M. More, G. R. Eaton, S. S. Eaton, *J. Am. Chem. Soc.* **1986**, *108*, 8194–8196.
[11] a) T. Mitsuma, *J. Phys. Soc. Jpn.* **1962**, *17*, 128–135; b) S. J. Tereniak, R. K. Carlson, L. J. Clouston, V. G. Young, E. Bill, R. Maurice, Y. S. Chen, H. J. Kim, L. Gagliardi, C. C. Lu, *J. Am. Chem. Soc.* **2014**, *136*, 1842–1855; c) B. A. Sastry, G. S. Sastry, *J. Chem. Phys.* **1973**, *59*, 6419–6423; d) V. S. X. Anthonisamy, M. Velayutham, R. Murugesan, *Physica B+C* **1999**, *262*, 13–19.
[12] a) S. Enthaler, X. F. Wu, M. Weidauer, E. Irran, P. Döhlert, *Inorg. Chem. Commun.* **2014**, *46*, 320–323; *##17##* b) A. T. Vallina, L. Leeren, Y. G. Li, O. Roubeau, R. Clérac, *Z. Anorg. Allg. Chem.* **2007**, *633*, 2400–2407.
[13] P. W. Anderson, *J. Phys. Soc. Jpn.* **1954**, *9*, 316–339.
[14] J. n. Titiš, R. Boča, *Inorg. Chem.* **2011**, *50*, 11838–11845.
[15] a) A. C. Rizzi, C. D. Brondino, R. Calvo, R. Baggio, M. T. Garland, R. E. Rapp, *Inorg. Chem.* **2003**, *42*, 4409–4416; b) N. I. Neuman, E. Winkler, O. Peña, M. C. G. Passeggi, A. C. Rizzi, C. D. Brondino, *Inorg. Chem.* **2014**, *53*, 2535–2544.
[16] a) V. Rosa, P. J. Gonzalez, T. Avilés, P. T. Gomes, R. Welter, A. C. Rizzi, M. C. Passeggi, C. D. Brondino, *Eur. J. Inorg. Chem.* **2006**, 4761–4769; b) A. Tamayo, J. Casabó, L. Escriche, P. González, C. Lodeiro, A. C. Rizzi, C. D. Brondino, M. C. G. Passeggi, R. Kivekäs, R. Sillanpää, *Inorg. Chem.* **2007**, *46*, 5665–5672.
[17] a) A. Goñi, L. Lezama, T. Rojo, M. Foglio, J. Valdivia, G. Barberis, *Phys. Rev. B* **1998**, *57*, 246–251; b) K. K. Mothilal, C. Karunakaran, P. Sambasiva Rao, R. Murugesan, *Spectrochim. Acta Part A* **2003**, *59*, 3337–3345.
[18] T. D. Smith, J. R. Pilbrow, *Coord. Chem. Rev.* **1974**, *13*, 173–278.
[19] J. M. Schveigkardt, A. C. Rizzi, O. E. Piro, E. E. Castellano, R. Costa de Santana, R. Calvo, C. D. Brondino, *Eur. J. Inorg. Chem.* **2002**, 2913–2919.
[20] P. W. Anderson, P. R. Weiss, *Rev. Mod. Phys.* **1953**, *25*, 269–276.
[21] N. I. Neuman, V. G. Franco, F. M. Ferroni, R. Baggio, M. C. G. Passeggi, A. C. Rizzi, C. D. Brondino, *J. Phys. Chem. A* **2012**, *116*, 12314–12320.
[22] a) A. L. Pérez, N. I. Neuman, R. Baggio, C. A. Ramos, S. D. Dalosto, A. C. Rizzi, C. D. Brondino, *Polyhedron* **2017**, *123*, 404–410; b) P. R. Levstein, H. M. Pastawski, J. L. D. Amato, *J. Phys. Condens. Matter* **1990**, *2*, 1781.
[23] O. Kahn, *Molecular Magnetism*, VCH Publishers; New York, **1993**.
[24] N. F. Chilton, R. P. Anderson, L. D. Turner, A. Soncini, K. S. Murray, *J. Comput. Chem.* **2013**, *34*, 1164–1175.
[25] a) J. Heyd, G. E. Scuseria, M. Ernzerhof, *J. Chem. Phys.* **2003**, *118*, 8207–8215; b) J. Heyd, G. E. Scuseria, M. Ernzerhof, *J. Chem. Phys.* **2006**, *124*, 219906; c) M. J. Frisch, G. W. Trucks, H. B. Schlegel, G. E. Scuseria, M. A. Robb, J. R. Cheeseman, G. Scalmani, V. Barone, B. Mennucci, G. A. Petersson, H. Nakatsuji, M. Caricato, X. Li, H. P. Hratchian, A. F. Izmaylov, J. Bloino, G. Zheng, J. L. Sonnenberg, M. Hada, M. Ehara, K. Toyota, R. Fukuda, J. Hasegawa, M. Ishida, T. Nakajima, Y. Honda, O. Kitao, H. Nakai, T. Vreven, J. A. Montgomery Jr., J. E. Peralta, F. Ogliaro, M. Bearpark, J. J. Heyd, E. Brothers, K. N. Kudin, V. N. Staroverov, R. Kobayashi, J. Normand, K. Raghavachari, A. Rendell, J. C. Burant, S. S. Iyengar, J. Tomasi, M. Cossi, N. Rega, J. M. Millam, M. Klene, J. E. Knox, J. B. Cross, V. Bakken, C. Adamo, J. Jaramillo, R. Gomperts, R. E. Stratmann, O. Yazyev, A. J. Austin, R. Cammi, C. Pomelli, J. W. Ochterski, R. L. Martin, K. Morokuma, V. G. Zakrzewski, G. A. Voth, P. Salvador, J. J. Dannenberg, S. Dapprich, A. D. Daniels, Ö. Farkas, J. B. Foresman, J. V. Ortiz, J. Cioslowski, D. J. Fox, *Gaussian 09, Revision C.1, Gaussian, Inc., Wallingford CT,* ***2009***.
[26] a) J. L. F. Da Silva, M. V. Ganduglia-Pirovano, J. Sauer, V. Bayer, G. Kresse, *Phys. Rev. B* **2007**, *75*, 045121; b) I. D. Prodan, G. E. Scuseria, R. L. Martin, *Phys. Rev. B* **2007**, *76*, 033101.

Received: May 14, 2018